Journal of
Applied
Crystallography

ISSN 0021-8898

Received 27 July 2012
Accepted 15 November 2012

High-pressure phase transitions and equations of state in NiSi. III. A new high-pressure phase of NiSi

Ian G. Wood,* Jabraan Ahmed, David P. Dobson and Lidunka Vočadlo

Department of Earth Sciences, University College London, Gower Street, London WC1E 6BT, England. Correspondence e-mail: ian.wood@ucl.ac.uk

A new high-pressure phase of NiSi has been synthesized in a multi-anvil press by quenching samples to room temperature from 1223–1310 K at 17.5 GPa and then recovering them to atmospheric pressure. The crystal structure of this recovered material has been determined from X-ray powder diffraction data; the resulting fractional coordinates are in good agreement with those obtained from an *ab initio* computer simulation. The structure, in which each atom is six-fold coordinated by atoms of the other kind, is orthorhombic (space group *Pmmn*) with $a = 3.27$, $b = 3.03$, $c = 4.70$ Å. This orthorhombic phase of NiSi may be considered as a ferroelastic distortion of the hypothetical tetragonal (space group *P*4/*nmm*) NiSi structure that was predicted to be the most stable phase (at 0 K) for pressures between 23 and 61 GPa in an earlier *ab initio* study by Vočadlo, Wood & Dobson [*J. Appl. Cryst.* (2012), **45**, 186–196]. Further *ab initio* simulations have now shown that, with increasing pressure (at 0 K), NiSi is predicted to exist in the following polymorphs: (i) the MnP structure; (ii) the new orthorhombic structure with space group *Pmmn*; and (iii) the CsCl structure. Experimentally, all of these structures have now been observed and, in addition, a fourth polymorph, an ε-FeSi-structured phase of NiSi (never the most thermodynamically stable phase in athermal *ab initio* simulations), may be readily synthesized at high pressure (P) and temperature (T). On the basis of both experiments and computer simulations it is therefore now clear that the phase diagram of NiSi at high P and T is complex. The simulated free-energy differences between different structures are often very small (<10 meV atom^{-1}) and there is also the possibility of two displacive ferroelastic phase transformations, the first between structures with *Pmmn* and *P*4/*nmm* symmetry, and the second from *P*4/*nmm* to a different orthorhombic phase of NiSi with space group *Pbma*. A complete understanding of the NiSi phase diagram (which may be of relevance to both planetary cores and the use of thin films of NiSi in semiconductor technology) can, therefore, only come *via in situ* experiments at simultaneous high P and high T.

1. Introduction

Nickel monosilicide (NiSi) is a most interesting material which, until very recently, had received little study under non-ambient conditions of pressure (P) and temperature (T). The ambient-pressure MnP-structured phase of NiSi (Toman, 1951) is of technological importance, as films of NiSi may be used in forming contacts in microelectronics, such as the connections to the source, drain and gate of CMOS devices (see *e.g.* Lavoie *et al.*, 2006). The crystal structure of this MnP-structured form of NiSi has space group *Pnma* and can be considered in terms of a distortion of the hexagonal NiAs structure (space group $P6_3/mmc$), with both Ni and Si in six-fold coordination: each Si atom is surrounded by six Ni atoms, forming a coordination polyhedron that is a distorted trigonal prism, and each Ni atom is surrounded by six Si atoms, located at the vertices of a distorted octahedron [see *e.g.* Fig. 4 of Vočadlo *et al.* (2012)]. Further details of previous investigations of the crystal structure of the MnP-structured phase of NiSi are given by Vočadlo *et al.* (2012). NiSi is known to behave in an unusual way at high temperature (but atmospheric pressure), showing 'enormous anisotropy' (Rabadanov & Ataev, 2002) in its thermal expansion, with the b axis of the crystal contracting strongly as the temperature is raised; this effect has been observed in both bulk samples (Wilson & Cavin, 1992; Rabadanov & Ataev, 2002; Perrin *et al.*, 2007, 2008) and thin films (Detavernier *et al.*, 2003).

Very recently, as part of an ongoing study of the role of (Fe,Ni)Si compounds in the cores of planetary bodies, we have investigated the properties of NiSi at high pressure. Initially this was done by athermal (effectively 0 K) *ab initio* computer simulations of the material (Vočadlo *et al.*, 2012), which revealed that the 0 K phase diagram of NiSi is much more

complicated than that of FeSi, with five phases being predicted to be stable for $P < 300$ GPa. The symmetries and structure types (where known) of these phases and the transition pressures between them were found to be as follows [see Vočadlo *et al.* (2012) for a full description]:

$$Pnma\,(\mathrm{MnP}) \leq 23\,\mathrm{GPa} \leq P4/nmm\,(\mathrm{CuTi}) \leq 61\,\mathrm{GPa} \leq Pbma\text{-I} \leq 168\,\mathrm{GPa} \leq Pnma\text{-III}\,(\mathrm{FeB}) \leq 247\,\mathrm{GPa} \leq Pm\bar{3}m\,(\mathrm{CsCl}). \quad (1)$$

A sixth phase, with the cubic ε-FeSi structure (space group $P2_13$; see *e.g.* Vočadlo *et al.*, 1999), was also found in these simulations to have only a marginally higher free energy (8–12 meV atom^{-1}) than the *Pbma*-I phase listed above, suggesting that it might be easily stabilized by temperature. A subsequent synchrotron X-ray diffraction study (Lord *et al.*, 2012) of quenched samples of NiSi produced by laser-heated diamond anvil cell (LHDAC) experiments then revealed transitions from ambient-pressure MnP-structured NiSi to the ε-FeSi structure (at 12.5 ± 4.5 GPa and 1550 ± 150 K) and thence to the CsCl structure (at 46 ± 3 GPa and 1900 ± 150 K). As predicted by the earlier computer simulations, the CsCl structure then remained the stable phase up to the highest pressure investigated (124 GPa). However, during this LHDAC study, weak peaks from minor phases were also observed in the diffraction patterns from some of the quenched samples, which suggested that it might also be possible for NiSi to crystallize in some of the other structures predicted by the *ab initio* simulations of Vočadlo *et al.* (2012). In particular, it seemed possible that the *P*4/*nmm* (CuTi) phase, predicted to be the most stable for $23 < P < 61$ GPa, might occur. It was also found in these experiments that the ε-FeSi-structured phase could be recovered on decompression to atmospheric pressure, but that the CsCl-structured phase could not.

The LHDAC experiments (Lord *et al.*, 2012) were designed to reach extremely high conditions of P and T to address the likely structure of NiSi within the deep Earth and planetary cores, and so were not really suitable for investigating the NiSi phase diagram at more modest pressures and temperatures. In particular, the minimum annealing temperature was ∼1400 K. Therefore, it was decided to carry out a further set of quenching experiments, in the range $0 < P < 20$ GPa and $1000 < T < 2200$ K using a multi-anvil press (MAP), by which to constrain this region of the NiSi phase diagram. During the course of these experiments we have discovered a new phase of NiSi with space group *Pmmn*, which we have found to be a ferroelastically distorted variant of the *P*4/*nmm* (CuTi) phase predicted in the *ab initio* simulations (Vočadlo *et al.*, 2012). A distortion of this kind was not considered in our earlier *ab initio* study. Therefore, in the present paper, as well as the experimental determination of the crystal structure, we also report the results of athermal *ab initio* simulations of this *Pmmn* phase, which we have found to have a lower free energy (by between ∼5 and ∼25 meV atom^{-1}, depending on the pressure) than the *P*4/*nmm* (CuTi), *Pbma*-I and *Pnma*-III (FeB) structures listed above. In §§2 and 3 we describe the experimental study; the methodology and results of the *ab initio* simulations are then given in §§4 and 5, with a brief general discussion in §6.

2. Experimental details

2.1. High-pressure sample synthesis

The high-pressure synthesis experiments were performed as follows. The sample of NiSi used in this investigation, prepared by arc melting at the ISIS Facility (Rutherford Appleton Laboratory, Didcot, Oxfordshire), was taken from the same batch of material as was used in the LHDAC study by Lord *et al.* (2012), where full details of its composition and characterization are given. The sample was found to be essentially phase pure by X-ray powder diffraction, with the composition of the bulk of the material found to be $Ni_{49.84\,(6)}Si_{50.16\,(6)}$ by energy-dispersive electron microprobe analysis. However, scanning electron microscopy and electron microprobe analysis did reveal that very minor regions of the sample showed Ni_3Si_2 stoichiometry, thought to originate from a very fine scale intergrowth of NiSi and δ-Ni_2Si [see Lord *et al.* (2012) for further details].

Powdered samples of this starting material were packed into 1.6 mm internal diameter alumina capsules for high-pressure sintering experiments using a 1000 tonne Walker-type multi-anvil press at University College London. The cell design is sketched in Fig. 1. The Cr-doped MgO octahedra had a 10 mm edge length and were compressed using tungsten carbide anvils with 4 mm truncations. Furnaces consisted of a single graphite cylinder (there is no transformation from graphite to diamond at the low temperatures of the present experiments, even at 18 GPa), and steel end-caps acted as electrical leads. A zirconia cylinder and end-plates provided thermal insulation. In the first experiment, a tungsten–rhenium (3/25Re) thermocouple was placed radially across the centre of the furnace, dividing the sample volume into two parts. One part contained

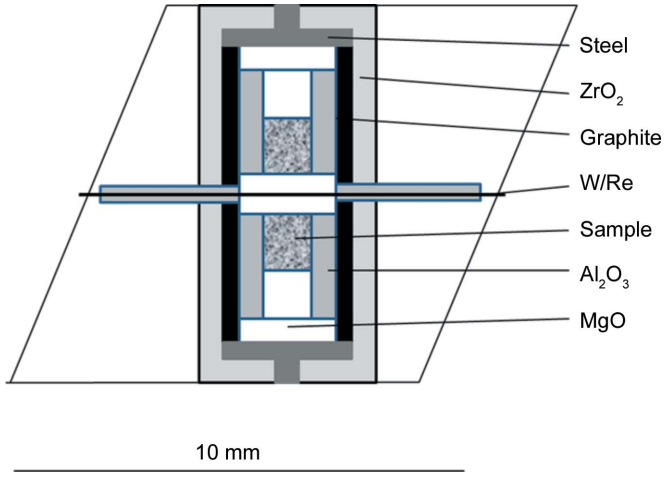

Figure 1
Sample assembly used in the high-P multi-anvil press. The outline of the Cr-doped MgO octahedron is shown; other components are as indicated. For further details see text.

NiSi, while the other contained Mg_2SiO_4 as a pressure calibrant: phase coexistence of β and γ phases of Mg_2SiO_4 constrained the pressure of the experiment to 17.5 GPa. Subsequent experiments used the pressure and temperature calibrations of the first experiment, thus maximizing the sample volume. Experience suggests that, for cell components machined in a single batch, temperature reproducibility is better than 50 K at 1273 K, and thermal gradients, estimated from finite difference models, are <100 K mm^{-1} in the central region of the furnace. No correction was applied to the thermocouple electromotive force for the effect of pressure, and quoted temperatures are for the hottest region of the furnace. Experiments were performed by compression to the desired end load at room temperature. The furnace was then heated to the required temperature and that temperature maintained for durations of 24 h or more at constant end load. At the end of the experiment the temperature was quenched by cutting electrical power to the furnace, resulting in quench rates of several hundred kelvin per second, and the pressure was then slowly released over a period of ~15 h.

An experiment carried out at 14 ± 1 GPa and 1270 ± 50 K led to a recovered sample containing two phases of NiSi: the room-pressure *Pnma* MnP-structured phase and that with the $P2_13$ ε-FeSi structure. In an attempt to obtain a pure sample of the ε-FeSi phase of NiSi, an experiment was then performed at 17.5 ± 1 GPa and 1310 ± 20 K. The product from this produced an X-ray diffraction pattern containing reflections from the ε-FeSi-structured phase, together with those from a material of unknown structure. The diffraction pattern from this new material showed features suggesting that it might be related to the *P*4/*nmm* (CuTi) phase predicted to occur in our earlier *ab initio* simulations. In particular, there was a strong reflection from the recovered sample with a *d* spacing of ~4.7 Å, characteristic of the *c* axis at $P = 0$ GPa [V_0 = 11.79 Å^3 atom^{-1}; see Fig. 2(*b*) of Vočadlo *et al.* (2012)]. This hypothesis suggested that the new material was likely to be the more stable phase at lower temperatures, so a final experiment was run at 17.5 ± 1 GPa and 1223 ± 50 K. The resulting sample still showed some peaks from the ε-FeSi structure but these were greatly reduced in intensity relative to those from the new material. Experiments at still lower temperatures were not run, as it was found that this sample, in combination with our later *ab initio* simulations (see §5), was sufficient to characterize the new material. It also seemed possible that, at temperatures much lower than 1200 K, the kinetics of the transformation might require an excessively long annealing time.

2.2. X-ray powder diffraction

The recovered sample from the MAP experiment at 17.5 GPa and 1223 K was in the form of a solid pellet of volume approximately 4.5 mm^3. This was broken free of the alumina sleeve and crushed gently under propanol in an agate pestle and mortar; excessive grinding was avoided in case it led to back transformation of the sample. Approximately 3 mm^3 of the resulting coarse powder was then dispersed in propanol on a 180 µm thick soda-glass plate (a microscope slide coverslip). Although it is difficult to avoid preferred orientation using this method, we have found it a very convenient way in which to mount small samples from the MAP for X-ray powder diffraction analysis, as it allows them to be readily examined with optical microscopes and easily recovered for other experiments. The powder diffraction measurement was then performed in Bragg–Brentano reflection geometry on a PANalytical X'Pert Pro diffractometer with Co $K\alpha_1$ radiation (40 kV, 30 mA), monochromated using an incident-beam focusing Ge(111) Johansson monochromator. The diffraction pattern was collected over the range $10 < 2\theta < 113^\circ$ with constant illumination of a 10×10 mm region of the sample; the data were then converted to fixed divergence slit geometry, using the software supplied by PANalytical, for the subsequent analysis (described in §3).

2.3. Electron-probe microanalysis

The remaining ~1.5 mm^3 of sample was mounted in cold-curing epoxy resin and polished, for analysis by scanning electron microscopy and electron microprobe. Back-scattered electron images of this sample, taken on a JEOL JSM-6480LV scanning electron microscope at an accelerating voltage of 15 kV, revealed the presence of two phases with subtle differences in their backscattered electron intensity. Subsequent examination using a JEOL JXA-8100 Superprobe in energy-dispersive mode (17 kV accelerating voltage, 9 nA beam current, and using elemental standards for Ni and Si) showed that the majority, darker, phase had a composition identical, within error, to the NiSi starting composition, whereas the other was more nickel rich, having a composition $Ni_{53}Si_{47}$. An estimate of the phase proportions was made from backscattered-electron images of the sample by thresholding on greyscale intensity and measuring the relative areas covered by the two nickel silicide phases using the *ImageJ* program (Abramoff *et al.*, 2004). The phase proportions found from this procedure (80% NiSi and 20% $Ni_{53}Si_{47}$ ±5%) were in reasonable agreement with those determined by X-ray diffraction (see §3).

3. Structure solution and refinement

Although it seemed likely that the material with unknown crystal structure produced in the experiments described above would be related to one of the phases examined in our previous *ab initio* simulations (Vočadlo *et al.*, 2012), it was decided to attempt to solve the structure *a priori* from the X-ray powder data, as this would reduce the possibility that our conclusion as to the likely atomic arrangement would be biased by our previous work.

Therefore, a Le Bail refinement (Le Bail *et al.*, 1988) of the data, as implemented in the *GSAS* suite of programs (Larson & Von Dreele, 1994; Toby, 2001), was first carried out, including the two phases known to be present, ε-FeSi-structured NiSi and α-alumina (from the sample capsule). The *d* spacings of nine reflections in the pattern at low 2θ angles, which could not be attributed to either of these phases, were

then input into the auto-indexing program *DICVOL06* (Boultif & Louër, 2004). This gave an orthorhombic solution with high figures of merit (M_9 = 260.3; F_9 = 123.4) and all lines indexed with low-integer Miller indices. The cell parameters from *DICVOL06* (a = 3.27, b = 3.03, c = 4.70 Å and V = 46.51 Å^3) were closely related to those of the *P*4/*nmm* tetragonal CuTi phase of NiSi predicted by Vočadlo *et al.* (2012) and the volume per atom (assuming Z = 2) was 11.63 Å^3. This value lies between that of the ambient-pressure MnP-structured phase (12.09 Å^3 atom^{-1}; Rabadanov & Ataev, 2002) and that of the ε-FeSi-structured phase recovered to atmospheric pressure (11.43 Å^3 atom^{-1}; Lord *et al.*, 2012), which was also strongly indicative of a correct solution.

The unit cell from *DICVOL06* was then used in a Le Bail refinement of the data to extract the values of the structure factors of the 34 Bragg reflections with the largest d spacings, and the crystal structure was determined by the Monte Carlo based simulated-annealing method using the program *Endeavour* (Putz *et al.*, 1999; Crystal Impact, 2010). Since the unit cell contained only four atoms it was not necessary to assume any symmetry during this process. *Endeavour* reproducibly found a solution with space group *Pmmn* (an obvious sub-group of *P*4/*nmm*), with atomic coordinates essentially identical to those predicted for the *P*4/*nmm* tetragonal phase of NiSi by Vočadlo *et al.* (2012). Both Ni and Si atoms lie on special positions in *Pmmn* of type 2*a*, at ($\frac{1}{4}$, $\frac{1}{4}$, z) [with respect to a unit cell chosen such that the origin is at a centre of symmetry; note also that, for direct compatibility with the corresponding tetragonal structure in space group *P*4/*nmm* (see below and §6), the 2*a* sites and not the 2*b* sites in *Pmmn* must be used].

Finally, the structures of both NiSi phases were refined by the Rietveld method, again as implemented within *GSAS*. Three phases were included in the refinement: α-alumina, ε-FeSi-structured NiSi and the *Pmmn* phase. Peak shape 4 was employed for all phases as there was obvious asymmetric line broadening in the latter. Preferred orientation corrections were refined using eighth-order spherical harmonic approximations for the two NiSi phases and a sixth-order approximation for the α-alumina, leading to texture coefficients of 1.10 for the alumina, 1.41 for the ε-FeSi-structured material and 1.73 for the *Pmmn* phase. The refined values of the mass fractions were 0.081 (2), 0.092 (2) and 0.828 (4), respectively, in agreement with the observations from the backscattering electron micrographs that the more electron dense ε-FeSi-structured material was the minor phase. For the α-alumina, the atomic coordinates and anisotropic displacement parameters were kept fixed at the single-crystal values listed by Thompson & Wood (1983), with only the cell parameters allowed to vary. For the two NiSi phases, the cell parameters, fractional coordinates and isotropic displacement parameters were refined. Since the data were not of the highest quality, it was decided to constrain the displacement parameters of the Ni and Si atoms to be equal to each other in both NiSi phases [the displacement parameters had previously been found to have similar values for the two atoms in ε-FeSi itself at room temperature; see Table 1(*a*) and Vočadlo *et al.* (2002)]. The structural parameters resulting from this fit are listed in Table 1 and the fitted diffraction pattern is shown in Fig. 2.[1] The χ^2 value for the fit was 6.37, with profile and weighted profile R factors of 0.063 and 0.087, respectively. A final Le Bail refinement of the data gave a χ^2 value of 6.17, very similar to that from the Rietveld refinement, indicating that the major sources of misfit originated from imperfections in the peak shapes and background, rather than from errors in the structures. In particular, as well as features associated with a slight mismatch of the observed and calculated peak shapes, the difference pattern shown in Fig. 2 has broad features, such as that found at about 2θ = 36.9°, which correspond to regions in which strong Bragg reflections from the ambient-pressure MnP-structured phase of NiSi would be expected. It seems likely, therefore, that these features arise from back transformation of a small part of the sample during its recovery from high pressure and grinding to produce the sample for X-ray diffraction.

Table 1
Structural parameters for NiSi polymorphs at P = 0.

Values in brackets are estimated standard uncertainties and refer to the least significant digit; where such values are listed for *ab initio* simulations they reflect only the uncertainties derived from fitting the *E versus V* points to an integrated Birch–Murnaghan third-order EoS. In the ε-FeSi structure (see *e.g.* Vočadlo *et al.*, 2002), both atoms lie on 4*a* (x, x, x) sites in space group $P2_13$. The *ab initio* values shown for NiSi in part (*a*) are those at V_0 [see Table 1 of Vočadlo *et al.* (2012)]. In the *Pmmn* structure both atoms lie on 2*a* ($\frac{1}{4}$, $\frac{1}{4}$, z) sites in space group *Pmmn* (with the origin chosen to lie on a centre of symmetry). The *ab initio* values in part (*b*) are those from a simulation made at V_0 (see §5.1).

(*a*) ε-FeSi phase of NiSi (values for ε-FeSi itself also shown for comparison).

	NiSi, present work	NiSi, *ab initio* (Vočadlo *et al.*, 2012)	FeSi, neutron diffraction (Vočadlo *et al.*, 2002)	FeSi, *ab initio* (Vočadlo *et al.*, 1999)
a (Å)	4.49678 (5)†	4.5265 (4)	4.48678 (1)	4.463
V (Å^3)	90.929 (3)	92.744 (24)	90.325 (1)	88.896
Ni x (Fe x)	0.1470 (9)	0.1479	0.13652 (5)	0.1367
U_{iso} (Å^2)	0.017 (2)‡		0.00292 (5)	
Si x	−0.1399 (12)	−0.1539	−0.15760 (9)	−0.1591
U_{iso} (Å^2)	0.017 (2)‡		0.00350 (12)	

(*b*) *Pmmn* phase of NiSi (all values are from the present work).

	Experimental values	*Ab initio* simulations
a (Å)	3.2735 (1)	3.2911
b (Å)	3.0266 (1)	3.0404
c (Å)	4.69776 (6)	4.7088
V (Å^3)	46.544 (1)	47.117
Ni z	0.3442 (2)	0.3412
U_{iso} (Å^2)	0.0200 (9)‡	
Si z	0.8423 (9)	0.8418
U_{iso} (Å^2)	0.0200 (9)‡	

† Lord *et al.* (2012) report a value of a = 4.5050 (5) Å for material produced in their LHDAC study and recovered to atmospheric pressure. ‡ Values constrained to be equal.

[1] Supplementary data for this paper are available from the IUCr electronic archives (Reference: KS5332). Services for accessing these data are described at the back of the journal.

A detailed discussion of the unusual sevenfold-coordinated ε-FeSi structure can be found in the articles by Vočadlo *et al.* (1999, 2000, 2002); this phase of NiSi was also discussed in some detail by Vočadlo *et al.* (2012) and Lord *et al.* (2012). Therefore, it is not discussed further here, except to remark that the cell and structural parameters shown in Table 1(*a*) are in reasonable agreement with those from previous work. The agreement between the fractional coordinates determined from our Rietveld refinement of this phase of NiSi and from our *ab initio* simulation is less good than in our previous studies of ε-FeSi itself. We consider this discrepancy, which almost certainly arises from the limitations of the present experiment, to be acceptable, bearing in mind that the experimental results are from a phase of NiSi that represented only 9 wt% of the sample and that the composition of this material was Ni rich (see §2.3).

Projections of the crystal structure of the new *Pmmn* phase of NiSi are shown in Fig. 3. The structure is essentially identical to that of the *P*4/*nmm* phase described by Vočadlo *et al.* (2012), which has the CuTi structure [Karlsson (1951); labelled B-11 in the *Strukturbericht* classification]; the relationship between the two, and to the *Pbma*-I structure described by Vočadlo *et al.* (2012), is discussed further in §6. The primary coordination of both types of atom in the *Pmmn* phase is identical, taking the form of an octahedron, one half of which is elongated parallel to [001] and the other half of which is shortened parallel to [001], as shown in Fig. 3(*c*). The six vertices of these octahedra are composed of atoms of the other kind to that lying within it. Thus, the primary coordination of each Ni atom is by six Si atoms at the octahedral vertices and *vice versa*. The crystal structure may then be considered in terms of an edge-sharing assemblage of either $NiSi_6$ or $SiNi_6$ octahedra. The atom within each octahedron is displaced parallel to [001] such that the distances to the vertices are fairly equal; these interatomic distances are 2.340 (4), 2.358 (4) and 4 × 2.395 (1) Å, irrespective of whether Ni or Si is taken to be the octahedrally coordinated species. Despite the lowering of symmetry from tetragonal to orthorhombic, four of the interatomic distances remain equal, as the octahedrally coordinated atoms (and the octahedron itself) are constrained to lie at the intersection of two mirror planes. The next-nearest-neighbour distances are very slightly different for the two species of atom: Ni has four next-nearest-neighbour Ni atoms at 2.667 (1) Å, with the five atoms lying at

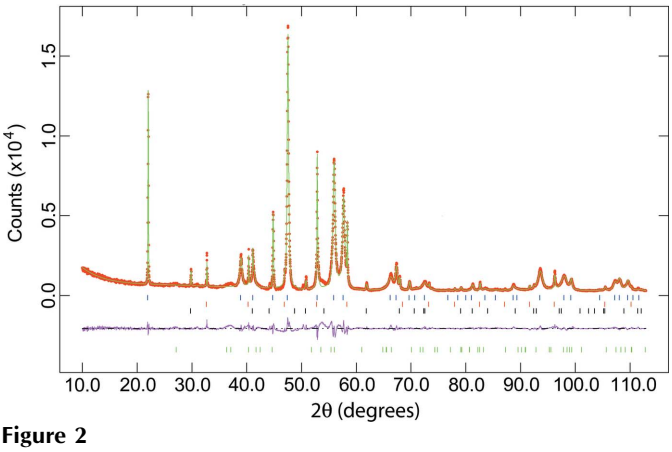

Figure 2
Observed (points), calculated (line) and difference (lower trace) X-ray powder diffraction pattern for Rietveld refinement of a sample of NiSi quenched from 1223 K at 17.5 GPa (for details, see text). The upper set of tick marks shows the positions of the Bragg reflections from (top downwards) NiSi in the *Pmmn* phase, NiSi in the ε-FeSi phase and α-Al_2O_3 (from the sample capsule). The broad features in the difference trace, for example at 37°, probably correspond to back transformation of some of the NiSi to its ambient-pressure MnP structure (see text); the reflection markers for this MnP-structured phase (which was not included in the refinement) are shown below the difference pattern.

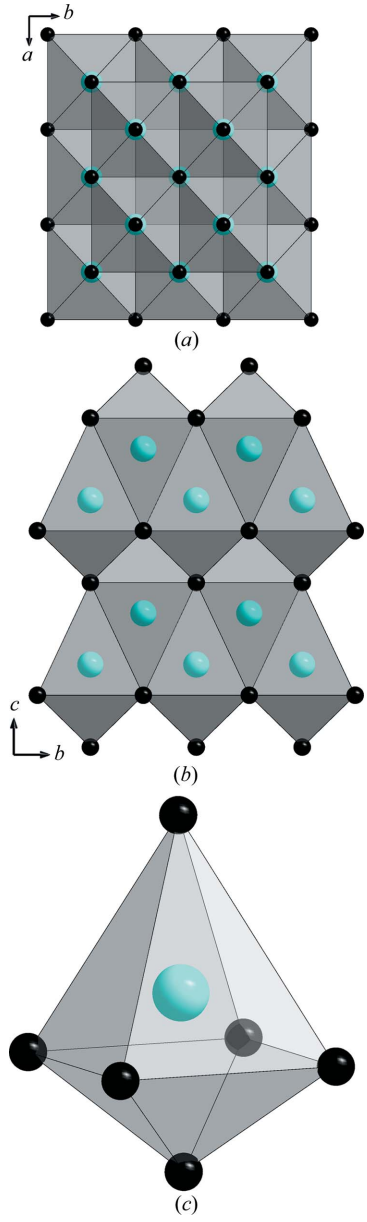

Figure 3
The crystal structure of the *Pmmn* phase of NiSi, as determined by X-ray powder diffraction. (*a*) A projection down [001]. (*b*) A projection down [100]. (*c*) The coordination polyhedron surrounding an Ni atom. The Si atoms are represented by small dark spheres. The symbols used are chosen to correspond to those used by Vočadlo *et al.* (2012) and their size is not intended to give a representation of the atomic displacement parameters.

Table 2
Equation-of-state parameters for the *Pmmn* phase of NiSi, obtained by fitting the internal energy *versus* volume from the *VASP* simulations to integrated third-order Birch–Murnaghan equations of state (EoSs).

Values in brackets are estimated standard uncertainties and refer to the least significant digit; they reflect only the uncertainties derived from fitting the *E versus V* points to the EoS.

V_0 (Å^3 atom^{-1})	K_0 (GPa)	K_0'	E_0 (eV atom^{-1})	Volume, pressure range fitted (Å^3 atom^{-1}, GPa)
11.7793 (5)	166.826 (3)	4.05 (8)	−5.84058 (1)	$10.75 < V < 12.0$, $18.4 > P > -3.0$
11.670 (6)	175.563 (5)	4.348 (8)	−5.8301 (8)	$6.5 < V < 10.5$, $375 > P > 23.3$

the vertices of a right rectangular pyramid; the Si atoms are similarly related to four next-nearest-neighbour Si atoms at 2.677 (4) Å. For both Ni and Si, the next-nearest-neighbour coordination is completed by four more atoms of the same kind, two at 3.0266 (1) Å and two at 3.2735 (2) Å.

However, probably the simplest way in which to visualize this structure is as a distorted form of that of NaCl, to which it may be transformed along a continuous pathway. If the z coordinates of the atoms are altered from those shown in Table 1(*b*) such that the Ni and Si atoms are placed at $(\frac{1}{4}, \frac{1}{4}, \frac{1}{4})$ and $(\frac{1}{4}, \frac{1}{4}, \frac{3}{4})$, and the cell parameters are made to take the form a, a, $2^{1/2}a$, the resulting structure is that of NaCl. Several transition metal nitrides have previously been reported to show this distortion of the NaCl structure to one of space group *Pmmn* [CrN (Nasr Eddine & Bertaut, 1971), $Cr_{1-x}V_xN$ (Nasr Eddine *et al.*, 1977) and $Cr_{1-x}Ti_xN$ (Nasr Eddine *et al.*, 1977)], but in these materials the distortion from cubic symmetry is much less than that found here for NiSi.

4. *Ab initio* simulations: methodology

4.1. Simulations of the new *Pmmn* phase of NiSi

The calculations were made using the method described in our earlier *ab initio* study of NiSi polymorphs (Vočadlo *et al.*, 2012). They are based on density functional theory (Hohenberg & Kohn, 1964) within the generalized gradient approximation (GGA; Wang & Perdew, 1991) implemented in the code *VASP* (Kresse & Furthmüller, 1996), with the projected augmented wave method (Blöchl, 1994; Kresse & Joubert, 1999) used to describe the electronic interactions with the atomic nuclei. The initial set of cell parameters and atomic coordinates for the *Pmmn* structure was taken from the experimental results shown in Table 1(*b*). The calculations were carried out using the primitive unit cell [as defined in Table 1(*b*)] and were performed with spin polarization, although no magnetic moments remained on the atoms after energy minimization. An energy cut off of 700 eV was used, together with an electronic minimization convergence criterion of 10^{-6} eV in the internal energy and an atomic minimization convergence criterion of 10^{-4} eV. In line with our previous calculations (Vočadlo *et al.*, 2012), a $13 \times 13 \times 13$ sampling grid in reciprocal space was used, leading to 343 k points in the symmetry-irreducible volume of the Brillouin zone. Calculation of the electronic density of states (DOS) was performed at intervals of approximately 0.104 eV in energy.

The equation-of-state (EoS) parameters shown in Table 2 were obtained by using *VASP* to calculate the internal energy (E) of the crystal at a set of chosen volumes (V), allowing both the cell parameters and the fractional coordinates to relax. During the calculations the program parameters were set such that the symmetry of the crystal was maintained and, therefore, phase transitions to structures with lower symmetry were forbidden. However, the converse is not true and a transition to the *P*4/*nmm* structure, the space group of which is a supergroup of *Pmmn*, would be allowed, as the atoms are not prevented from moving into a more symmetrical arrangement. The $E(V)$ curve was then fitted to an integrated Birch–Murnaghan third-order EoS, which was used to calculate the enthalpy H (see *e.g.* Vočadlo *et al.*, 1999, 2012). Since $T = 0$, the enthalpy is equal to the Gibbs free energy, G, and thus the most stable phase at any given pressure may be determined.

4.2. Simulations of an NiSi phase with tetrahedrally coordinated Ni

In order to extend our survey of possible structure types, some simulations were also made for NiSi in the tetragonal tetrahedrally coordinated layered FeSe structure (Hägg & Kindström, 1933). This structure (labelled B-10 in the *Strukturbericht* classification) can also be adopted by compounds such as FeS (Berner, 1962), for which it occurs naturally as the mineral mackinawite (*e.g.* Lennie *et al.*, 1995). Recently, materials of this type have attracted interest as high-T_c superconductors and because they show a number of structural and magnetic transitions at low temperatures and high pressures (see *e.g.* Margadonna *et al.*, 2009; Pan *et al.*, 2011). The starting coordinates for this NiSi simulation were taken from those reported for FeSe in space group *P*4/*nmm* by Pan *et al.* (2011); the other simulation parameters required for *VASP* were set at the values given above. Two spin polarization simulations were made, one with a starting configuration in which the magnetic moments on the Ni atoms were parallel (*i.e.* ferromagnetic) and one in which they were antiparallel (antiferromagnetic). These converged to the same internal energy, with no magnetic moments remaining on the atoms after energy minimization.

5. *Ab initio* simulations: results

5.1. Simulations of the new *Pmmn* phase of NiSi

Fig. 4(*a*) shows the unit-cell parameters from *VASP* for the *Pmmn* phase of NiSi as a function of simulation volume (V).[2] It can be seen that the structure remains orthorhombic

[2] The data used to plot Fig. 4 are available as part of the supplementary material for this paper.

throughout this range. Comparison of the calculated internal energies of the *Pmmn* phase of NiSi with those presented in Fig. 1 of Vočadlo *et al.* (2012) reveals that, at all volumes, the internal energy is slightly lower than that of either the *Pbma*-I or the *P*4/*nmm* structures considered in our earlier work and thus there is no transition to a higher-symmetry tetragonal structure, although for volumes greater than that for which $P = 0$ ($V > \sim 11.78$ Å^3 atom^{-1}, see below), *i.e.* for negative pressures, the crystal is clearly tending towards becoming tetragonal. There are inflections in all three of the lattice parameter *versus* volume plots shown in Fig. 4(*a*) (most easily seen for *a* and *b*) in the region $10.5 < V < 10.75$ Å^3 atom^{-1}, but these features are much smaller in magnitude than the discontinuities observed for some structures in our previous simulations of NiSi phases (Vočadlo *et al.*, 2012). The *z* coordinates of the Ni and Si atoms are shown in Figs. 4(*b*) and 4(*c*), respectively; it can be seen that these show little change, varying smoothly with simulation volume, though a slight alteration in the slope of the plots at a point corresponding to the inflection in the cell parameters can be clearly seen.

Because of the behaviour shown by the cell parameters, it was decided to fit separate equations of state to the $E(V)$ values on each side of the inflection. The resulting Birch–Murnaghan third-order EoS parameters are listed in Table 2. Fig. 5 [largely taken from Vočadlo *et al.* (2012)] shows the difference in enthalpy between each of the relevant phases of NiSi and that of NiSi in the CsCl structure [note that (i) as in the previous paper, those phases not shown in Fig. 5 all had enthalpies high enough to make them always thermodynamically unstable; (ii) use of a single EoS for the *Pmmn* phase gave an enthalpy difference curve that was almost identical to that shown in the figure, differing by <2 meV atom^{-1} in the pressure range of interest, *i.e.* for $P <$ 264 GPa]. From Fig. 5 it can be seen that the phases of NiSi expected to be thermodynamically stable at 0 K and the pressure ranges over which they occur are now somewhat different from those suggested previously, being (i) the MnP structure (as observed experimentally), $0 < P < \sim 21$ GPa; (ii) the new structure with space group *Pmmn*, $\sim 21 < P < \sim 264$ GPa; (iii) the CsCl structure, $P > \sim 264$ GPa. However, Fig. 5 also shows that, depending on the pressure, the free-energy difference between several of these structures can be very small, often <10 meV atom^{-1}. The consequence of this for the NiSi phase diagram is discussed further in §6.

The second column in Table 1(*b*) shows the results of a simulation carried out at the value of V_0 listed in the first row of Table 2 (*i.e.* at $P = 0$). It can be seen that, allowing for the slight inflation of the structure commonly found in *ab initio* simulations made using the GGA, the cell parameters correspond very well to those determined from our Rietveld refinement. The fractional coordinates are also in excellent agreement with our experimentally determined structure, differing by only 0.0030 and 0.0005 for Ni and Si, respectively.

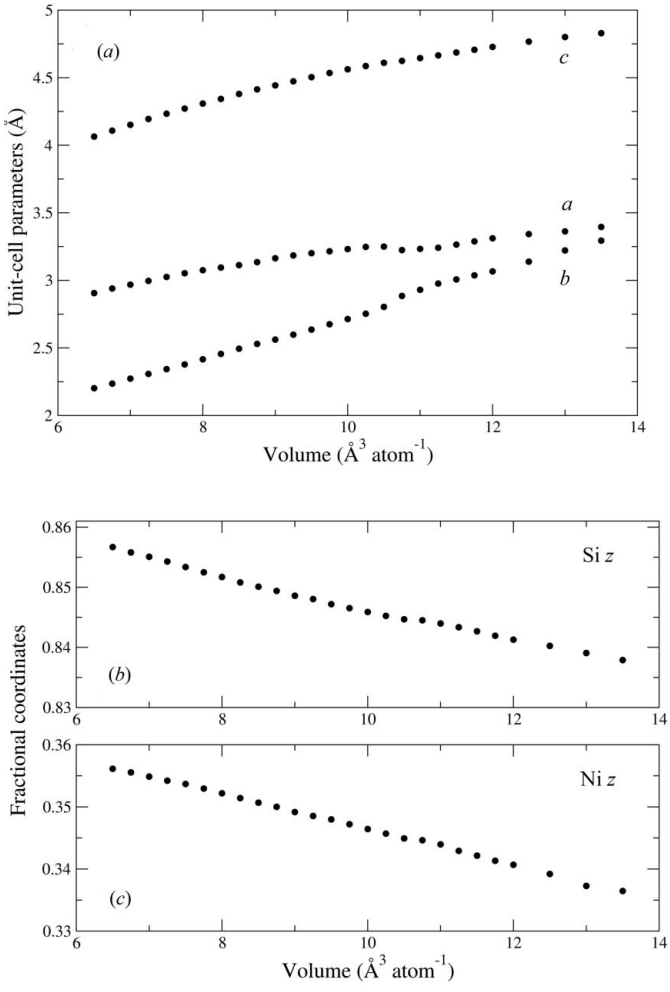

Figure 4
(*a*) Unit-cell parameters and (*b*), (*c*) atomic fractional *z* coordinates of the *Pmmn* phase of NiSi, as determined from the *VASP* simulations.

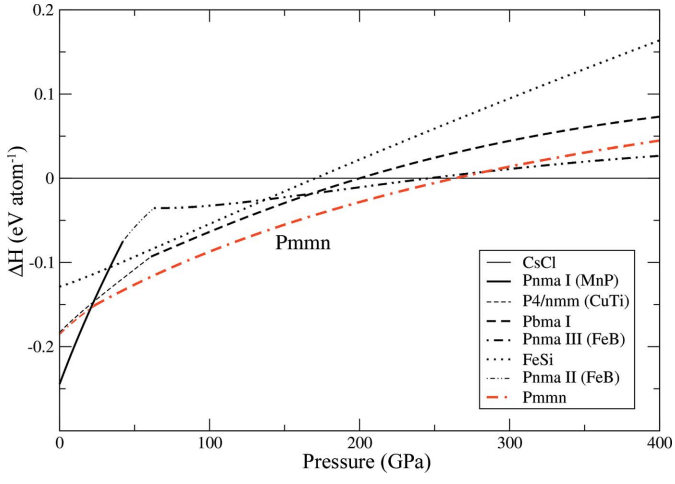

Figure 5
Enthalpy (here equal to Gibbs free energy) of NiSi phases from athermal *VASP* simulations as a function of pressure, relative to that of the CsCl structure. The enthalpy curves shown are identical to those given in Fig. 3 of Vočadlo *et al.* (2012), with the curve for the new *Pmmn* phase added (thick dot–dashed line; shown in red in the electronic version of the journal). With increasing pressure the sequence of stable phases of NiSi is now MnP structured → *Pmmn* phase → CsCl structured, with transition pressures of 21 and 264 GPa, respectively. Note, however, that the free-energy difference between many of the structures is only ∼5–25 meV atom^{-1}.

This good agreement with experiment strongly indicates that conclusions based on our simulations are likely to be robust.

The calculated electronic DOS of this material is shown in Fig. 6. It can be seen that, in common with the other phases of NiSi simulated in our earlier study (Vočadlo *et al.*, 2012), it is metallic but with the Fermi energy lying fairly close to a minimum in the DOS. The form of the DOS is not dissimilar to that of the ambient-pressure MnP phase of NiSi [see Fig. 7(*a*) of Vočadlo *et al.* (2012); note that when making this comparison it should be remembered that the simulation box used for the MnP phase contained twice as many atoms as that used here].

5.2. Simulations of NiSi with the tetrahedrally coordinated FeSe structure

Although we have not attempted to make a comprehensive study of possible tetrahedrally coordinated phases of NiSi, we briefly report here the results of our simulations of a hypothetical NiSi phase having the layered tetrahedrally coordinated FeSe structure (Pan *et al.*, 2011). This structure has the same space group, *P*4/*nmm*, as one of the hypothetical phases of NiSi considered in our previous study (Vočadlo *et al.*, 2012) but the atomic arrangement is quite different. For $V \geq 15$ Å^3 atom^{-1}, the internal energy converged to a value similar to that found for NiSi in the NaCl structure [see Fig. 1 of Vočadlo *et al.* (2012)], and thus much higher than that for any of the polymorphs found to be thermodynamically stable in our earlier study, with the slope of the $E(V)$ curve indicating that the material was under negative pressure. For $V \leq 14$ Å^3 atom^{-1}, the simulations resulted in a transition to the CsCl structure, requiring large displacements of the Si atoms in the simulation box (their z coordinates changed from $\sim\pm0.23$ to 0.5) and a cell with a c/a ratio of $1/(2^{1/2})$. On the basis of these simulations, it therefore seems clear that (except, perhaps, for a hypothetical region of the phase diagram for which $P < 0$) tetrahedrally coordinated structures of this type are most unlikely ever to form the thermodynamically stable phase of NiSi. This result is not unexpected, since all the structures that were found to be stable in our previous simulations (Vočadlo *et al.*, 2012), our previous experiments (Lord *et al.*, 2012) and the present work have coordination numbers for both atoms of six or higher (see §6).

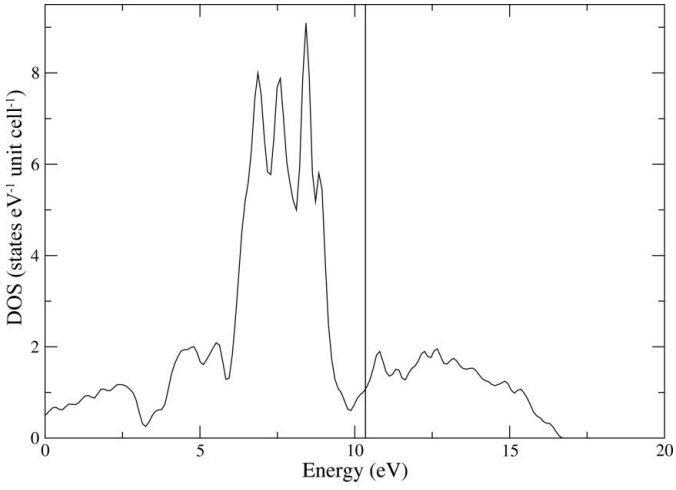

Figure 6
Total electronic density of states for the *Pmmn* phase of NiSi from a *VASP* simulation. The calculation was made at the zero-pressure simulation volume of 11.7793 Å^3 atom^{-1}. The vertical line shows the position of the Fermi energy.

6. Discussion

Although we have not yet been able to prepare an entirely single-phase sample of the orthorhombic *Pmmn* phase of NiSi described here, we believe that our experimental and computational results, taken together, provide very strong evidence that this is the stable phase of NiSi at low to moderate temperature (*e.g.* $T < \sim1100$ K) and $P \sim17.5$ GPa. Our MAP experiments at this pressure showed an increasing amount of this material relative to the cubic ε-FeSi-structured phase as the temperature was reduced from 1310 to 1223 K, and our *ab initio* simulations indicate that it becomes the thermodynamically stable phase of NiSi at 0 K for $P > 21$ GPa. Similarly, although our powder data were necessarily compromised by the limited amount of sample available (and by line broadening at higher Bragg angles), the good agreement between the experimental and computational crystal structures listed in Table 1(*b*) suggests that our experimental determination of the fractional coordinates is reliable. The study presented here and the work described in our earlier papers on NiSi (Vočadlo *et al.*, 2012; Lord *et al.*, 2012) therefore illustrate very well the power of combining experimental work with *ab initio* computer simulations. Initially, simulations provided the basis for the LHDAC study; more recently, our MAP experiments have provided the stimulus for further computational work.

If the enthalpy-difference plots shown in Fig. 5 of the present paper are compared with those shown in Fig. 3 of our earlier publication (Vočadlo *et al.*, 2012), it might at first be thought that the revised phase diagram for NiSi implied by Fig. 5 is somewhat simpler. In fact, the opposite is almost certainly true. Since our *VASP* simulations were athermal, the results shown in Fig. 5 effectively define a phase diagram at 0 K, but whether this predicted sequence of phases remains at higher temperatures will depend on the Clapeyron slopes of the phase boundaries. Thus, for example, we have shown in both our LHDAC and MAP experiments that the cubic ε-FeSi-structured phase of NiSi is readily made, despite it never being the most thermodynamically stable phase at any pressure in our athermal simulations. The enthalpy differences between several of the different structures shown in Fig. 5 are so small ($\sim$10 meV atom^{-1}; 10 meV = 116 K) that they may be easily overcome at moderate temperatures. This is especially true for the structure reported here and those discovered and labelled *Pbma*-I and *P*4/*nmm* (CuTi) in our earlier computer simulations (Vočadlo *et al.*, 2012). The space groups *Pmmn* and *Pbma* are both subgroups of *P*4/*nmm* and it is thus possible to envisage these orthorhombic phases as being

formed by ferroelastic distortions of a hypothetical (at present) form of NiSi with space group *P*4/*nmm*. Both distortions are of ferroelastic species 4/*mmmFmmm* (Aizu, 1969). The structure with *Pmmn* symmetry is formed from the tetragonal phase by retention of glide/mirror planes perpendicular to [001] and ⟨100⟩, accompanied by loss of the fourfold axis and any planes of symmetry perpendicular to ⟨110⟩. Essentially, the only difference between the two structures is that the *ab* cross section of the unit cell in the orthorhombic phase is slightly distorted from square to rectangular [see Fig. 3 of the present paper and Fig. 8(*b*) of Vočadlo *et al.* (2012)]. The structure with *Pbma* symmetry is formed by retention of glide/mirror planes perpendicular to [001] and ⟨110⟩, accompanied by loss of the fourfold axis and any planes of symmetry perpendicular to ⟨100⟩. In this case, as shown in Fig. 8(*a*) of Vočadlo *et al.* (2012), there is also a decrease in translational symmetry, with the unit cell doubling in volume, with $a_{\rm O} \simeq b_{\rm O} = 2^{1/2}a_{\rm T}$ and $a_{\rm O} = c_{\rm T}$ (where the subscripts O and T refer to the orthorhombic and tetragonal phases, respectively). Finally, in connection with this discussion of the formation of lower-symmetry phases of NiSi by ferroelastic distortions, it should be mentioned that the space group *P*4/*nmm* is itself a subgroup of $Fm\overline{3}m$, *i.e.* of the space group of the NaCl structure type from which this form of NiSi may be considered to be derived (see §3 and Fig. 3). However, *ab initio* simulations have shown that NaCl-structured NiSi has a considerably higher internal energy than the other polymorphs investigated [see Fig. 1 of Vočadlo *et al.* (2012)].

Since, in the present study, we only have diffraction patterns from samples quenched in *T* and then recovered from high *P* to ambient *P*, it is not possible to deduce whether NiSi adopts the structure with *Pmmn* symmetry under the conditions at which this phase was formed, *i.e.* at 17.5 GPa and 1223 K, or whether this structure arises as the result of a displacive ferroelastic phase transformation from the higher-symmetry phase with *P*4/*nmm* symmetry. Our *ab initio* simulations [see Fig. 4 of this paper and Fig. 2(*b*) of Vočadlo *et al.* (2012)] strongly indicate that the stability of both orthorhombic phases increases relative to that of the *P*4/*nmm* parent phase as *P* is increased. However, an orthorhombic–tetragonal transition might occur at high temperature, as suggested by the facts that a *Pbma* to *P*4/*nmm* transition was observed as the simulation volume was increased (*i.e.* as *P* was reduced) in our previous computational study [see Fig. 2(*b*) of Vočadlo *et al.* (2012)] and that in the present work a tendency towards the tetragonal structure is observed when the *Pmmn* phase is simulated under conditions corresponding to negative pressure (*i.e.* for $V > \sim 11.78$ Å^3 atom^{-1}; Fig. 4*a*). Thus, depending upon the conditions of *P* and *T*, it seems quite possible that a transition to the tetragonal *P*4/*nmm* phase of NiSi will be observed and it is also possible that the *Pbma* distortion of this structure may have a region of phase stability. These issues, together with the exact phase fields of the different structures, can only be resolved by *in situ* experiments at simultaneous high *P* and high *T*. However, such studies would not be without difficulties, as the pressure range required extends beyond the upper limit of that routinely attainable with MAPs, whereas the temperature range required lies between that attainable in DACs by external heating and by laser heating.

The question remains as to whether the phases of NiSi discussed here and in our previous papers (Vočadlo *et al.*, 2012; Lord *et al.*, 2012) are the only polymorphs of NiSi that are likely to exist in the range of pressure and temperature that we have investigated. The fact that we have good agreement between the structure types observed experimentally (MnP, orthorhombically distorted CuTi, ε-FeSi and CsCl) and those predicted to be the most stable in our computer simulations (MnP, orthorhombically distorted CuTi and CsCl) suggests that we may now have the complete set of relevant NiSi structure types. The fact that the primary coordination number of the atoms in the stable polymorph increases with pressure, from six (in the MnP and orthorhombically distorted CuTi structures) to seven (ε-FeSi) to eight (CsCl), further suggests that (at least for $P \geq 0$) tetrahedrally coordinated structures – a possibility that we have not considered in detail (see §5.2) – are unlikely to lead to phases that are ever thermodynamically the most stable. However, these arguments may not necessarily be true, especially as the structures that were examined in our computer simulations were all derived from either known structure types or simple modifications thereof obtained by interchange of atoms. Since the methodology used in the simulations allows phase transitions to supergroups of the starting space group to occur, but not to subgroups, some possible structures may have been missed. Indeed, this was the case for the structure with *Pmmn* symmetry reported here, as this distortion of the structure with *P*4/*nmm* symmetry was simply not considered in our earlier work, one reason being that it seemed to be more likely that the higher-symmetry tetragonal structure would be the stable phase at moderate pressure, rather than any of its orthorhombic distortions [as was indicated by the orthorhombic to tetragonal phase transition found to occur in our previous study as the simulation volume was increased; see Fig. 2(*b*) of Vočadlo *et al.* (2012)]. To ensure that no other possibly stable hypothetical phases exist, it might therefore be fruitful to apply one of the automated approaches to structure prediction to this system, such as those using evolutionary algorithms or *ab initio* random structure searching.

It is clear from the results reported here and in our earlier papers (Vočadlo *et al.*, 2012; Lord *et al.*, 2012) that further experimental work is required to determine the NiSi phase diagram below ∼20 GPa, as this information could have implications both for planetary sciences and for understanding the formation of NiSi thin films in semiconductor devices. Within the Earth, it is to be expected that NiSi would adopt the high-*P* CsCl structure throughout most of the mantle and the entirety of the core (Lord *et al.*, 2012), but the same is not true for smaller bodies such as Mars, where the core–mantle boundary is expected to occur at ∼24 GPa (*e.g.* Bertka & Fei, 1997), or Mercury, in which the large core results in a core–mantle boundary pressure that may be as low as ∼4 GPa (*e.g.* Michel *et al.*, 2012). Transitions between the phases of NiSi at relatively low pressures (*e.g.* $P < 40$ GPa) may therefore have consequences for layering within the solid component of small

planetary cores. The transitions within the solid phases of NiSi are also likely to be reflected in alterations in the slope of the liquidus and will thus affect the position of inner–outer core boundaries. In this context NiSi, *per se*, must be viewed as one of the end-member compositions within the Fe–Ni–Si ternary system, and similar investigations of this ternary phase diagram across this pressure range are also required to determine, for example, the effect of the addition of iron on the relative stability of the three phases of NiSi that are now known to occur for $P < \sim 20$ GPa (*i.e.* that reported here and those with the MnP and ε-FeSi structures) or the effect of the addition of nickel on the transition between the ε- and CsCl-structured forms of FeSi. Although detailed investigations of the Fe–Ni–Si ternary system across a wide composition range at atmospheric pressure have been published (*e.g.* Ackerbauer *et al.*, 2009), similar studies at high pressure are sparse and have been limited to the study of very Fe rich alloys at very high pressures, being directed towards understanding the crystal structures (*e.g.* Sakai *et al.*, 2011), melting temperature (*e.g.* Morard *et al.*, 2011) and equations of state (*e.g.* Asanuma *et al.*, 2011) of materials within the Earth's core.

We believe that the discovery that two high-pressure phases of NiSi can be formed below ~17.5 GPa may also have some relevance to the study of the formation of the NiSi thin films that are used to form electrical contacts in semiconductor devices. For FeSi, it is well known that thin films of this material with the high-pressure CsCl-type structure can form on Si(111) substrates (von Känel *et al.*, 1992, 1994; Kafader *et al.*, 1993), despite the fact that, at the temperatures at which these films are grown (300–800 K), pressures well in excess of 20 GPa are required to produce this phase in a bulk sample (Dobson *et al.*, 2002; Lord *et al.*, 2010). Similarly, films of CoSi in the high-P CsCl structure have also been reported, grown on Si(111) substrates (von Känel *et al.*, 1995). In the case of NiSi, when thin films are grown on either Si(100) or Si(111) substrates by annealing a deposited layer of either Ni or Ni/Si, there is strong evidence that the resulting film – provided that the annealing has gone to completion – consists of NiSi with the room-pressure MnP structure (*e.g.* d'Heurle *et al.*, 1984), although the thermal-expansion mismatch between film and substrate may then result in the film being under a residual stress that is estimated to be between ~650 and ~1150 MPa (Murray *et al.*, 2009). However, during the annealing process, transient phases are also formed (d'Heurle *et al.*, 1984; De Keyser *et al.*, 2008; Van Bockstael *et al.*, 2009), the nature of which is still under investigation. To date, these transient phases have been analysed in terms of other Ni_xSi_y phases that are known to exist at atmospheric pressure, in particular δ-Ni_2Si, θ-Ni_2Si, Ni_3Si_2 and $Ni_{31}Si_{12}$ (Hoummada *et al.*, 2010). It seems clear from recent atom probe tomography microscopy (Hoummada *et al.*, 2010) that at least some of these transient phases are indeed nickel rich and related to the hexagonal θ-Ni_2Si structure (De Keyser *et al.*, 2008; Van Bockstael *et al.*, 2009), but it should be noted that the X-ray diffraction patterns shown by De Keyser *et al.* (2008) and Van Bockstael *et al.* (2009) to illustrate the formation of transient phases cover regions of reciprocal space in which strong Bragg reflections will be found both from the ε-FeSi-structured phase of NiSi and from the phase of NiSi with space group *Pmmn* described in the present paper. Thus, although we have no conclusive evidence that these high-pressure structures are in any way related to the transient phases seen during NiSi thin-film formation, we believe that this possibility (which has not been considered previously) should not be dismissed out of hand, since it is clear from previous work on FeSi and CoSi (see above) that epitaxial growth can lead to the formation of films with crystal structures requiring similarly high pressures for bulk synthesis.

7. Conclusions

A new high-pressure orthorhombic phase of NiSi has been synthesized at $P \simeq 17.5$ GPa. The crystal structure of this material, as determined from a sample recovered to room pressure and temperature, has space group *Pmmn*, with both Ni and Si atoms octahedrally coordinated by six atoms of the other species. This new NiSi polymorph forms at similar pressures, but lower temperatures, to the cubic ε-FeSi-structured phase of NiSi discovered by Lord *et al.* (2012). These experimental observations agree well with those expected from athermal *ab initio* simulations, which indicate that, at 0 K, the new polymorph will be the stable phase of NiSi for $21 < P < 264$ GPa. As observed experimentally, it should therefore be found at lower temperatures than the ε-FeSi-structured polymorph, which is then stabilized at higher T *via* the entropic contribution to the Gibbs free energy. The experiments presented here cannot rule out the possibility that the structure of the new form of NiSi, as it exists at high P and T, may be tetragonal (with space group $P4/nmm$), and that the recovered orthorhombic material has formed by a small ferroelastic distortion on quenching. This issue, together with the detailed location of the boundaries between the NiSi phases, can only be addressed by *in situ* studies at simultaneous high P and high T. We believe that such studies would be highly desirable, bearing in mind the role of Fe–Ni–Si alloys in small planetary cores and the possible significance of high-pressure phases of NiSi in understanding the formation of the technologically important thin films of NiSi on Si that are used to form contacts in semiconductor devices.

The authors thank Dr Devashibhai Adroja and Dr Kevin Knight (ISIS Facility, Rutherford Appleton Laboratory, England) for assistance with the sample preparation, and Dr Wilson Crichton (European Synchrotron Radiation Facility, Grenoble, France) for helpful discussions regarding possible tetrahedrally coordinated forms of NiSi.

References

Abramoff, M. D., Magalhaes, P. J. & Ram, S. J. (2004). *Biophotonics Int.* **11**, 36–42.
Ackerbauer, S., Krendelsberger, N., Weitzer, F., Hiebl, K. & Schuster, J. C. (2009). *Intermetallics*, **17**, 414–420.
Aizu, K. (1969). *J. Phys. Soc. Jpn*, **27**, 387–396.
Asanuma, H., Ohtani, E., Sakai, T., Terasaki, H., Kamada, S., Hirao, N. & Ohishi, Y. (2011). *Earth Planet. Sci. Lett.* **310**, 113–118.

Berner, R. A. (1962). *Science*, **137**, 669.
Bertka, C. M. & Fei, Y. (1997). *J. Geophys. Res.* **102**, 5251–5264.
Blöchl, P. E. (1994). *Phys. Rev. B*, **50**, 17953–17979.
Boultif, A. & Louër, D. (2004). *J. Appl. Cryst.* **37**, 724–731.
Crystal Impact (2010). *Endeavour*. Crystal Impact GbR, Bonn, Germany. http://crystalimpact.com/endeavour.
De Keyser, K., Van Bockstael, C., Detavernier, C., Van Meirhaeghe, R. L., Jordan-Sweet, J. & Lavoie, C. (2008). *Electrochem. Solid State Lett.* **11**, H266–H268.
Detavernier, C., Lavoie, C. & d'Heurle, F. M. (2003). *J. Appl. Phys.* **93**, 2510–2515.
Dobson, D. P., Vočadlo, L. & Wood, I. G. (2002). *Am. Mineral.* **87**, 784–787.
Eddine, M. N., Bertaut, E. F., Roubin, M. & Paris, J. (1977). *Acta Cryst.* B**33**, 3010–3013.
Hägg, G. & Kindström, A.-L. (1933). *Z. Phys. Chem. B*, **22**, 453–464.
d'Heurle, F., Petersson, C. S., Baglin, J. E. E., La Placa, S. J. & Wong, C. Y. (1984). *J. Appl. Phys.* **55**, 4208–4218.
Hohenberg, P. & Kohn, W. (1964). *Phys. Rev.* **136**, B864–B871.
Hoummada, K., Blum, D., Mangelinck, D. & Portavoce, A. (2010). *Appl. Phys. Lett.* **96**, 261904.
Kafader, U., Tuilier, M. H., Pirri, C., Wetzel, P., Gewinner, G., Bolmont, D., Heckmann, O., Chandesris, D. & Magnan, H. (1993). *Europhys. Lett.* **22**, 529–535.
Känel, H. von, Mäder, K. A., Müller, E., Onda, N. & Sirringhaus, H. (1992). *Phys. Rev. B*, **45**, 13807–13810.
Känel, H. von, Mendik, M., Mäder, K. A., Onda, N., Goncalves-Conto, S., Schwarz, C., Malegori, G., Miglio, L. & Marabelli, F. (1994). *Phys. Rev. B*, **50**, 3570–3576.
Känel, H. von, Schwarz, C., Goncalves-Conto, S., Müller, E., Miglio, L., Tavazza, F. & Malegori, G. (1995). *Phys. Rev. Lett.* **74**, 1163–1166.
Karlsson, N. (1951). *J. Inst. Met.* **79**, 391–405.
Kresse, G. & Furthmüller, J. (1996). *Phys. Rev. B*, **54**, 11169–11186.
Kresse, G. & Joubert, D. (1999). *Phys. Rev. B*, **59**, 1758–1775.
Larson, A. C. & Von Dreele, R. B. (1994). *GSAS*. Report LAUR 86-748. Los Alamos National Laboratory, New Mexico, USA.
Lavoie, C., Detavernier, C., Cabral, C., d'Heurle, F. M., Kellock, A. J., Jordan-Sweet, J. & Harper, J. M. E. (2006). *Microelectron. Eng.* **83**, 2042–2054.
Le Bail, A., Duroy, H. & Fourquet, J. L. (1988). *Mater. Res. Bull.* **23**, 447–452.
Lennie, A. R., Redfern, S. A. T., Schofield, P. F. & Vaughan, D. J. (1995). *Mineral. Mag.* **59**, 677–683.
Lord, O. T., Vočadlo, L., Wood, I. G., Dobson, D. P., Clark, S. M. & Walter, M. J. (2012). *J. Appl. Cryst.* **45**, 726–737.
Lord, O. T., Walter, M. J., Dobson, D. P., Armstrong, L., Clark, S. M. & Kleppe, A. (2010). *J. Geophys. Res.* **115**, B06208.
Margadonna, S., Takabayahi, Y., Ohishi, Y., Mizuguchi, Y., Takano, Y., Kagayama, T., Nakagawa, T., Takata, M. & Prassides, K. (2009). *Phys. Rev. B*, **80**, 064506.
Michel, N. C., Hauck, S. A., Solomon, S. C., Phillips, R. J., Roberts, J. H. & Zuber, M. T. (2012). 43rd Lunar and Planetary Science Conference, March 2012, Houston, Texas, USA, Abstract 1671.
Morard, G., Andrault, D., Guignot, N., Siebert, J., Garbarino, G. & Antonangeli, D. (2011). *Phys. Chem. Miner.* **38**, 767–776.
Murray, C. E., Zhang, Z. & Lavoie, C. (2009). *J. Appl. Phys.* **106**, 073521.
Nasr Eddine, M. & Bertaut, E. F. (1971). *Solid State Commun.* **9**, 717–723.
Nasr Eddine, M., Roubin, M. & Pâris, J. (1977). *Solid State Commun.* **32**, 953–954.
Pan, M., Ma, H. F., Zhu, J. T., Cheng, C. H., Huang, Zh., Zhang, Y., Zhang, H. & Zhao, Y. (2011). *Physica C*, **471**, 603–607.
Perrin, C., Mangelinck, D., Nemouchi, F., Labar, J., Lavoie, C., Bergman, C. & Gas, P. (2008). *Mater. Sci. Eng. B*, **154–155**, 163–167.
Perrin, C., Nemouchi, F., Clugnet, G. & Mangelinck, D. (2007). *J. Appl. Phys.* **101**, 073512.
Putz, H., Schön, J. C. & Jansen, M. (1999). *J. Appl. Cryst.* **32**, 864–870.
Rabadanov, M. Kh. & Ataev, M. B. (2002). *Crystallogr. Rep.* **47**, 40–45.
Sakai, T., Ohtani, E., Hirao, N. & Ohishi, Y. (2011). *Geophys. Res. Lett.* **38**, L09302.
Thompson, P. & Wood, I. G. (1983). *J. Appl. Cryst.* **16**, 458–472.
Toby, B. H. (2001). *J. Appl. Cryst.* **34**, 210–213.
Toman, K. (1951). *Acta Cryst.* **4**, 462–464.
Van Bockstael, C., De Keyser, K., Van Meirhaeghe, R. L., Detavernier, C., Jordan-Sweet, J. & Lavoie, C. (2009). *Appl. Phys. Lett.* **94**, 033504.
Vočadlo, L., Knight, K. S., Price, G. D. & Wood, I. G. (2002). *Phys. Chem. Miner.* **29**, 132–139.
Vočadlo, L., Price, G. D. & Wood, I. G. (1999). *Acta Cryst.* B**55**, 484–493.
Vočadlo, L., Price, G. D. & Wood, I. G. (2000). *Acta Cryst.* B**56**, 369–376.
Vočadlo, L., Wood, I. G. & Dobson, D. P. (2012). *J. Appl. Cryst.* **45**, 186–196.
Wang, Y. & Perdew, J. (1991). *Phys. Rev. B*, **44**, 13298–13307.
Wilson, D. F. & Cavin, O. B. (1992). *Scr. Metall. Mater.* **26**, 85–88.